Accelerated battery lifetime simulations using adaptive inter-cycle extrapolation algorithm

Valentin Sulzer[†], Peyman Mohtat , Sravan Pannala , Jason B. Siegel , and Anna G. Stefanopoulou

University of Michigan, Ann Arbor, MI, USA
[†] vsulzer@umich.edu

Abstract

We propose algorithms to speed up physics-based battery lifetime simulations by one to two orders of magnitude compared to the state-of-the-art. First, we propose a reformulation of the Single Particle Model with side reactions to remove algebraic equations and hence reduce stiffness, with 3x speed-up in simulation time (intra-cycle reformulation). Second, we introduce an algorithm that makes use of the difference between the 'fast' timescale of battery cycling and the 'slow' timescale of battery degradation by adaptively selecting and simulating representative cycles, skipping other cycles, and hence requires fewer cycle simulations to simulate the entire lifetime (adaptive inter-cycle extrapolation). This algorithm is demonstrated with a specific degradation mechanism but can be applied to various models of aging phenomena. In the particular case study considered, simulations of the entire lifetime are performed in under 5 seconds. This opens the possibility for much faster and more accurate model development, testing, and comparison with experimental data.

1 Introduction

Improved understanding of battery degradation will lead to better reliability, safety, extended utilization of batteries, and hence reduced costs [1]. Batteries for light duty vehicles and grid applications are made to last and warranted for 8-10 years [2, 3]. Battery degradation could therefore take around 10 years in the field, which is prohibitively long for understanding the effect of a battery design parameter change on lifetime. The total testing time is usually reduced in the lab by using accelerated aging conditions and skipping rest between cycles, degrading the battery in a few months. To reduce the time further, modeling is required. In particular, physics-based electrochemical models that embed degradation mechanisms are useful for evaluating the capacity and power fade of lithium-ion batteries under various duty cycles, and hence predicting their lifetime, since they can directly simulate a wide range of realistic battery uses at various scales [4]. However, physics-based simulations of the entire battery lifetime typically take several minutes to hours. For example, if a simulation of one full charge/discharge cycle takes one second, simulating 1000 cycles would take around 15 minutes. This is much faster than experimental timescales, but still too slow and not ideal for rapid feedback and repeated simulations of the model, for example in a parameter estimation routine which require multiple forward solves of the model. In this paper, we propose an algorithm to speed up physics-based battery lifetime simulations by one to two orders of magnitude, and hence simulate the entire lifetime of a battery in just a few seconds (Table 1).

Many modeling studies investigate the degradation for a single cycle, and there have been significant advances in performing simulations of individual cycles (intra-cycle simulations) as efficiently as possible. Smith et al. proposed a low order dynamic model with applications in battery management [5]. Cai et al. derived a reduced-order model using proper orthogonal decomposition [6]. Northrop et

	One full equivalent cycle	Lifetime
Battery lifetime	1 week	8-10 years
Lab experiments	2 hours	3 months
Standard SPM	0.6 seconds	10 minutes
SPM with intra-cycle reformulation (Section 3)	0.2 seconds	3 minutes
Reformulated SPM with adaptive inter-cycle extrapolation (Section 4)	0.2 seconds	5 seconds

Table 1: Order-of-magnitude timescales required to measure or simulate a single cycle or the entire lifetime of a battery. For 'battery lifetime' we assume a typical driving pattern and the industry-standard eight-year warranty. This can be reduced by continuously cycling the cell in the lab, and further reduced using simulations. For example, simulating one full cycle of the Single Particle Model (SPM) takes 0.6 seconds, so simulating the full lifetime (1000 cycles) takes around 10 minutes. This can be reduced to 0.2 seconds/ 3 minutes by reformulating the model to eliminate an algebraic equation (intra-cycle reformulation, Section 3). Without further changing the simulation time for one cycle, we further reduce the lifetime simulation time to under 5 seconds by adaptively extrapolating between cycles (inter-cycle extrapolation, Section 4).

al. reformulated the model for implementation in a battery management system [7], based on earlier work by Subramanian et al. [8]. Barai et al. proposed a reduced order model for mechanical degradation [9]. Two other very popular reduced-order models are the Single Particle Model [10] and Single Particle Model with electrolyte [11]. More recently, various authors have used perturbation theory to derive reduced-order one-dimensional [12, 13, 14, 15, 16] and three-dimensional [17, 18] models in a variety of asymptotic limits.

In comparison, few methods to accelerate simulations over the entire battery life have been proposed in the literature. The idea of using a detailed microscale simulation to inform a macroscale simulation without explicitly deriving the macroscale equations is relatively well-known [19, 20]. More rigorously, systems with distinct timescales can be solved asymptotically using the method of multiple scales [21]. Battery simulations are ideally suited to this approach, since they have a fast cycling timescale and a slow degradation timescale, and the fast timescale is usually periodic when performing controlled experiments in a laboratory setting [1]. However, to our knowledge, few studies have attempted to separate the cycling and degradation timescales.

One suggested algorithm is to iteratively simulate one cycle and linearly extrapolate the degradation over a fixed number of cycles (inter-cycle extrapolation). This algorithm was first proposed for fuel cell models by Mayur et al. [22, 23] as the 'time-upscaling method', and adapted to lithium-ion batteries by Kupper et al. [24]. Independently, Vora et al. [25] proposed a similar algorithm and called it 'extrapolation'. This fixed-size linear extrapolation algorithm has two major downsides, and has not gained wide-spread traction so far. First, the 'extrapolation' hyper-parameter needs to be selected a priori, with no systematic way of knowing an appropriate value. Second, the method takes fixed steps over the entire battery life, but some regions may require smaller steps and others larger steps depending on the linearity of aging.

In this paper, we propose an adaptive inter-cycle extrapolation algorithm where the step size is chosen automatically based on the past and present degradation rates. This algorithm works with any degradation model based on porous-electrode theory, but for presentation purposes we use a Single Particle Model with SEI growth and particle cracking, introduced in Section 2. We use different degradation parameters to simulate different capacity fade trajectories (linear, self-limiting, and accelerating). In Section 3, we show how the intra-cycle model can be reformulated to eliminate algebraic equations, for a 3x speed-up at almost no loss of accuracy. In Section 4, we introduce the adaptive inter-cycle extrapolation algorithm, and show results in each of the three degradation cases. In each case we achieve a further one to two order of magnitude speed-ups compared to the baseline. Since the speed-up combines multiplicatively with speed-ups in simulation of a single cycle, the entire lifetime of the battery can be simulated in just a few seconds. This enables interactions with the simulations

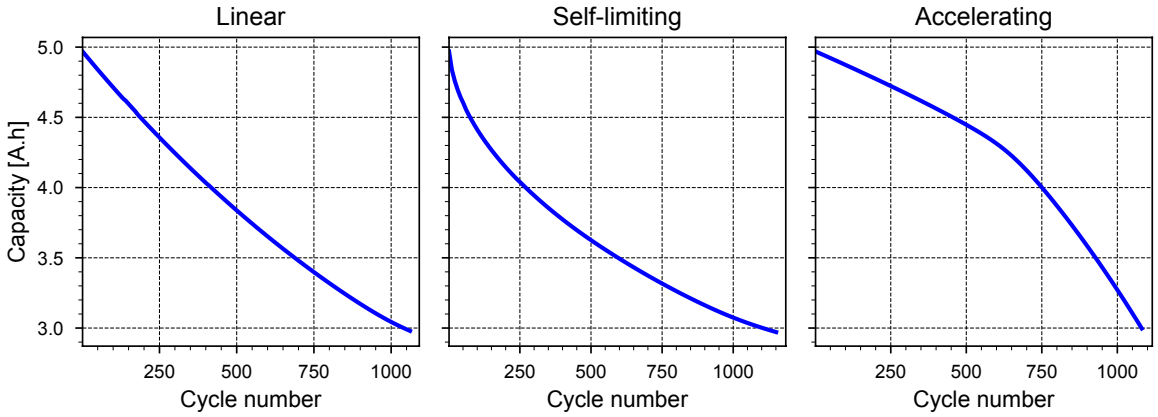

Figure 1: Different capacity fade trajectories with the parameters in Table 3.

on a human timescale [26], and therefore opens the possibility for much faster and more accurate model development and comparison with experimental data. The algorithm is implemented in the open-source battery modeling package PyBaMM [27] and thus can easily be used to simulate any aging model implemented within that framework. Alternatively, it can easily be incorporated in other simulation frameworks. The results presented in Section 4.3 also demonstrate how the capacity fade curve changes qualitatively when different degradation mechanisms dominate, as shown in Figure 1. In particular, we investigate the knee point around cycle 600 in the 'accelerating' capacity fade curve, and show that this knee point is caused by electrode saturation. Finally, several extensions and possible research directions enabled by this algorithm are discussed in Section 5.

2 Degradation model

The algorithms introduced in this work are intended to be general and work with any degradation model based on porous-electrode theory. For demonstration purposes, we will show the numerical improvements which are the main focus of the paper in a case study degradation model, namely the Single Particle Model with SEI formation [28] and loss of active material [29, 30] due to particle swelling [31, 32]. More complicated models can also be used without modification to the algorithms that we introduce below. The case study degradation model is as follows:

Single Particle Model:

$$\frac{\partial c_{\mathrm{s},k}}{\partial t} = \frac{1}{r^2}\frac{\partial}{\partial r}\left(r^2 \frac{\partial c_{\mathrm{s},k}}{\partial r}\right), \qquad 0 < r < R_k, \tag{1a}$$

$$\frac{\partial c_{\mathrm{s},k}}{\partial r} = -\frac{j_{\mathrm{int},k}}{F}, \qquad r = R_k. \tag{1b}$$

SEI model [28]:

$$j_{\text{int},k} = 2i_0 \sinh\left(\frac{F\eta_k}{2RT}\right), \tag{1c}$$

$$j_{\text{SEI}} = f_{\text{SEI}}(\eta_{\text{SEI}}, \delta_{\text{SEI}}), \tag{1d}$$

$$\frac{\text{I}}{a_{\text{s,n}} L_{\text{n}}} = j_{\text{tot,n}} = j_{\text{int,n}} + j_{\text{SEI}}, \tag{1e}$$

$$\eta_{\text{n}} = \phi_{\text{s,n}} - \phi_{\text{e}} - U_{\text{n}}(c^{\text{surf}}_{\text{s,n}}) - j_{\text{tot,n}} R_{\text{film}} \delta_{\text{SEI}}, \tag{1f}$$

$$\eta_{\text{SEI}} = \phi_{\text{s,n}} - \phi_{\text{e}} - U_{\text{SEI}} - j_{\text{tot},k} R_{\text{film}} \delta_{\text{SEI}}, \tag{1g}$$

$$\frac{\text{d}\delta_{\text{SEI}}}{\text{d}t} = \bar{V}_{\text{SEI}} \frac{a_{\text{s,n}} j_{\text{SEI}}}{2F}. \tag{1h}$$

$$\eta_{\text{p}} = \phi_{\text{s,p}} - \phi_{\text{e}} - U_{\text{p}}(c^{\text{surf}}_{\text{s,p}}), \tag{1i}$$

$$-\frac{\text{I}}{a_{\text{s,p}} L_{\text{p}}} = j_{\text{tot,p}} = j_{\text{int,p}}, \tag{1j}$$

where f_{SEI} is a function derived in Appendix A. Particle mechanics, assuming maximum stress at the particle surface and zero minimum stress [29, 30, 31, 32]:

$$\sigma_{\text{h},k} = \frac{2\Omega_k E_k}{3(1-\nu_k)} \left(\frac{1}{R_k^3} \int_0^{R_k} c_{\text{s},k} r^2 \, \text{d}r - c^{\text{surf}}_{\text{s},k} \right), \tag{1k}$$

$$\frac{\text{d}\varepsilon_{\text{s},k}}{\text{d}t} = \beta_{\text{LAM}} \left(\frac{\sigma_{\text{h},k}}{\sigma_k^{\text{critical}}} \right)^{m_{\text{LAM}}}, \tag{1l}$$

$$a_{\text{s},k} = \frac{3\varepsilon_{\text{s},k}}{R_k}, \tag{1m}$$

Voltage:

$$V = U_{\text{p}}(c^{\text{surf}}_{\text{s,p}}) - U_{\text{n}}(c^{\text{surf}}_{\text{s,n}}) + \eta_{\text{p}} - \eta_{\text{n}}. \tag{1n}$$

Parameter values are as in [32] with additional degradation parameters given in Table 2. After spatial discretization (for example using finite volumes), the discretized state vector is

$$\boldsymbol{x} = [\boldsymbol{c}_{\text{s,n}}, \boldsymbol{c}_{\text{s,p}}, \delta_{\text{SEI}}, \varepsilon_{\text{s,n}}, \varepsilon_{\text{s,p}}]^T. \tag{2}$$

The degradation rate can be controlled by tuning three parameters k_{SEI}, D_{SEI}, and β_{LAM}. We demonstrate the fast simulation algorithm in three scenarios with qualitatively different degradation paths: one linear, one self-limiting, and one accelerating (Figure 1). The parameters that result in these three behaviors are given in Table 3. In each case, we simulate the entire lifetime using both standard sequential cycle simulations and adaptive inter-cycle extrapolation, and compare the results. Each cycle consists of a 1 C discharge until 3 V, followed by 1 hour rest, then 1 C charge until 4.2 V, and finally 4.2 V hold until the current goes below C/50. Simulations are performed until 60% capacity fade, with capacity defined by equation (26) derived in Appendix B. The capacity fade curves in Figure 1 are obtained by solving the model (1) in PyBaMM [27], using the Metohd of Lines to semi-discretize the PDEs and SUNDIALS (via CasADi) [33, 34] to solve the resulting system of ODEs/DAEs. Each cycle is simply initialized with the final state of the previous cycle,

$$\boldsymbol{x}_0^k = \boldsymbol{x}_{\text{end}}^{k-1}. \tag{3}$$

Parameter	Meaning	Value		Reference
		neg	pos	
$c_{\text{EC}}^{\text{bulk}}$	Concentration of EC in bulk electrolyte [mol/m^3]	4541	-	[35]
V_{SEI}	SEI molar volume [m^3/mol]	9.585×10^{-5}	-	[35]
α_{SEI}	SEI charge transfer coefficient [-]	0.5	-	[35]
δ_{SEI}^0	Initial SEI thickness [m]	5×10^{-9}	-	[35]
R_{SEI}	SEI resistivity [Ωm]	2×10^{5}	-	[35]
E_k	Young's modulus [Pa]	15×10^9	375×10^9	[31]
ν_k	Poisson ratio [-]	0.2	0.3	[31]
Ω_k	Partial molar volume of solute [m^3/mol]	3.1×10^{-6}	-7.28×10^{-7}	[31]
$\sigma_k^{\text{critical}}$	Critical stress [Pa]	60×10^6	375×10^6	(†)
m_{LAM}	LAM exponent [-]	2	2	(†)

Table 2: Degradation parameters of the model. Other parameters are as in [32]. The three remaining degradation parameters are different for each case as shown in Table 3. (†) parameter introduced in this paper.

Parameter	Meaning	Linear	Self-limiting	Accelerating
k_{SEI}	SEI kinetic rate constant [m/s]	1×10^{-15}	1×10^{-14}	1×10^{-17}
D_{SEI}	SEI layer diffusivity [m^2/s]	2×10^{-16}	5×10^{-20}	2×10^{-18}
β_{LAM}	Cracking rate [1/s]	1.7×10^{-7}	1.4×10^{-8}	1.9×10^{-6}

Table 3: Key degradation parameters for each type of degradation. Parameters were selected to show the required capacity fade trajectory with 60% capacity fade in around 1000 cycles.

3 Intra-cycle model reformulation of side reactions

One way to accelerate lifetime simulations is to make the simulation of individual cycles faster, either through model reformulation, reduced-order models, or more efficient numerical algorithms. Here, we propose a model reformulation for side reactions that can eliminate an algebraic equation from the model, and achieves a 3x speed-up compared to the original model. After spatial discretization, the reformulated model is an ODE system (instead of a DAE system for the original model), which enables the use of a wider range of algorithms from control theory.

3.1 Model reformulation

Equations (1c)-(1g) can be collapsed into a single algebraic equation for the surface potential difference $\phi_{\text{s,n}} - \phi_{\text{e}}$,

$$\frac{\text{I}}{a_{\text{n}} L_{\text{n}}} = 2i_0 \sinh\left(\frac{F}{2RT}\left(\phi_{\text{s,n}} - \phi_{\text{e}} - U_{\text{n}}(c_{\text{s,n}}^{\text{surf}}) - j_{\text{tot,n}} R_{\text{film}} \delta_{\text{SEI}}\right)\right) - f_{\text{SEI}}(\phi_{\text{s,n}} - \phi_{\text{e}} - U_{\text{SEI}} - j_{\text{tot},k} R_{\text{film}} \delta_{\text{SEI}}, \delta_{\text{SEI}}). \quad (4)$$

Without side reactions, and assuming symmetric Butler-Volmer as is usually the case, the potentials can then be found in closed form by inverting the Butler-Volmer equation. When side reactions are included, no closed form solutions exist for the transcendental equations of the form (4), and so (4) is an additional algebraic equation that must be solved alongside the other equations of the model (diffusion in the particles, in the case of the SPM). This turns the model from an ODE system to a DAE system after semi-discretization, and hence requires more complex and slower numerical methods to solve.

To avoid this issue, the model can be reformulated by exploiting the fact that the side reaction current density is much smaller than the intercalation current density [29]. Systematically performing

the asymptotic expansion requires a full non-dimensionalization and is beyond the scope of this paper, but the general idea is as follows. We note that the size of the SEI current is much smaller than the size of the intercalation current and define some small parameter $\varepsilon \ll 1$, such that $j_{\text{SEI}}/j_{\text{int}}$ $\mathcal{O}(\varepsilon)$. We also define $g_{\text{SEI}} = f_{\text{SEI}}/\varepsilon$ to be $\mathcal{O}(1)$. We then expand kinetics variables in powers of ε,

$$j_{\text{int}} = j_{\text{int}}^0 + \varepsilon j_{\text{int}}^1 + \dots, \tag{5a}$$
$$j_{\text{SEI}} = j_{\text{SEI}}^0 + \varepsilon j_{\text{SEI}}^1 + \dots, \tag{5b}$$
$$\eta = \eta^0 + \varepsilon \eta^1 + \dots, \tag{5c}$$
$$\eta_{\text{SEI}} = \eta_{\text{SEI}}^0 + \varepsilon \eta_{\text{SEI}}^1 + \dots. \tag{5d}$$

Substituting (5) into 1c-1g, we find that to leading order in ε,

$$\eta^0 = \frac{2RT}{F} \sinh^{-1}\left(\frac{j_{\text{int}}^0}{2i_0}\right), \tag{6a}$$
$$j_{\text{SEI}}^0 = 0, \tag{6b}$$
$$j_{\text{int}}^0 = j_{\text{tot}}. \tag{6c}$$

To first order in ε,

$$j_{\text{SEI}}^1 = g_{\text{SEI}}^0 = -f_{\text{SEI}}(\eta_{\text{SEI}}^0, \delta_{\text{SEI}})/\varepsilon, \tag{7a}$$
$$j_{\text{int}}^1 = -j_{\text{SEI}}^1, \tag{7b}$$

and so we have an explicit approximate form for j,

$$j_{\text{int}} \approx j_{\text{int}}^0 + \varepsilon j_{\text{int}}^1 = j_{\text{tot}} + f_{\text{SEI}}\left(\eta^0 + U(c_{\text{s}}) - U_{\text{SEI}}, \delta_{\text{SEI}}\right), \tag{8}$$

where η^0 is given by (6a). We then directly use the explicit form (8) in the boundary condition for the particle diffusion equation, (28b), so that loss of lithium inventory during cycling is accounted for as in Appendix C. With this approach, the model remains a system of ODEs; compared to the standard SPM, the only additional equation is equation (1h) for the SEI thickness growth, and there are no additional equations for the current. The derivation is very similar if other side reactions, such as lithium plating, are included. However, this approach breaks down if side reactions begin to dominate, since the asymptotic expansion is no longer valid.

Note that the simplification from DAE to ODE only works if the Butler-Volmer reaction is symmetric, since it relies on inverting the sinh term. In the case of non-symmetric Butler-Volmer reactions, an alternative way to keep the model as an ODE system is to introduce capacitance into the system, for example in the form

$$C_{\text{dl}} \frac{\partial}{\partial t}\left(\phi_{\text{s}} - \phi_{\text{e}}\right) = j_{\text{tot}} - j_{\text{int}} - j_{\text{SEI}}, \tag{9}$$

where C_{dl} is the double-layer capacitance [36, 37].

Furthermore, the simplification from DAE to ODE is only applicable for electrode-averaged models such as the Single Particle Model. In the full DFN model [12], the total interfacial current j_{tot} is not simply given by (1e), but instead is spatially distributed in the electrode and must be solved for in an algebraic equation.

3.2 Results

We now compare the model with ODE formulation (8) and DAE formulation (1c)-(1g) for the SEI equations, over one representative 1C/1C discharge/charge cycle. We compare the relevant electrical variables in Figure 2: voltage, V, total interfacial current density in the negative electrode, $j_{\text{tot,n}}$, intercalation current density in the negative electrode, $j_{\text{int,n}}$, SEI overpotential, η_{SEI}, SEI current

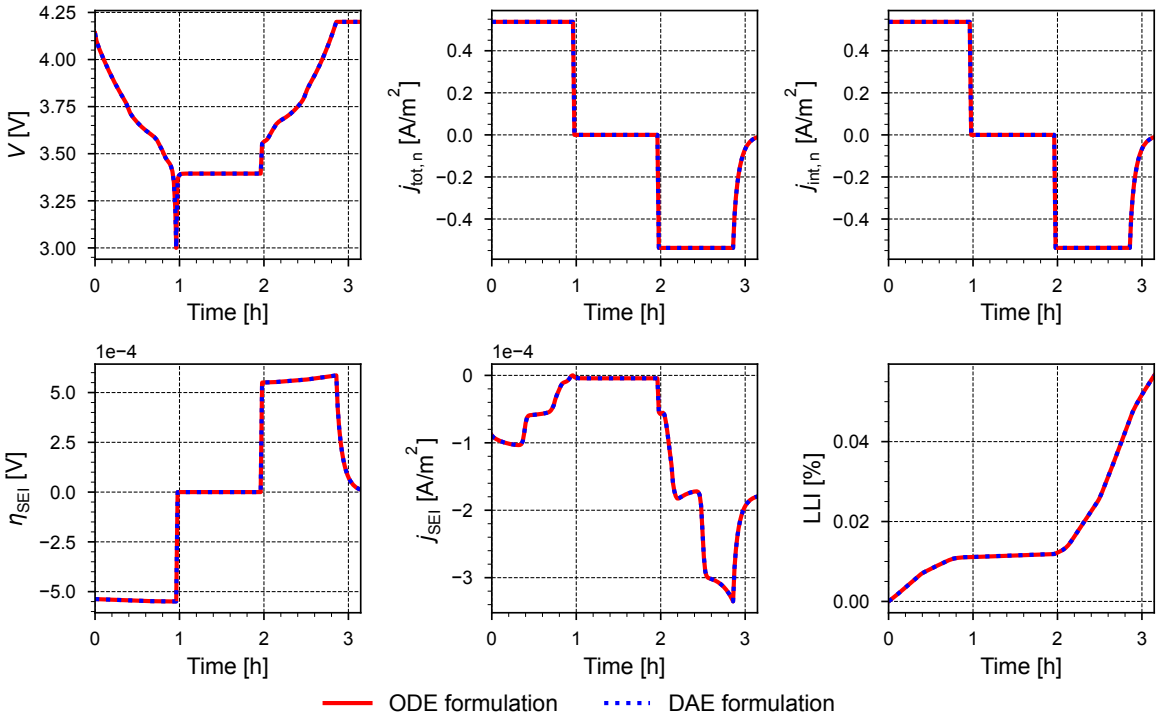

Figure 2: Comparison of the ODE formulation (8) and DAE formulation (1c)-(1g) for the SEI equations. Both formulations are simulated using PyBaMM [27].

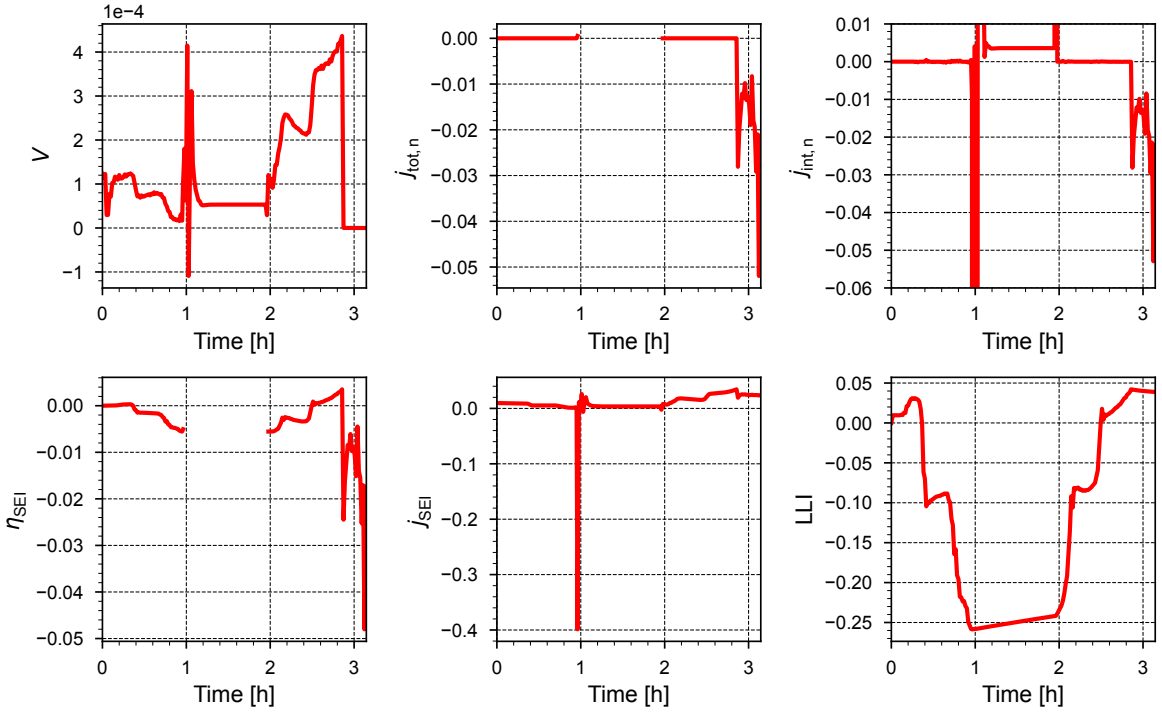

Figure 3: Root mean square percentage error between the ODE formulation (8) and DAE formulation (1c)-(1g) for the SEI equations.

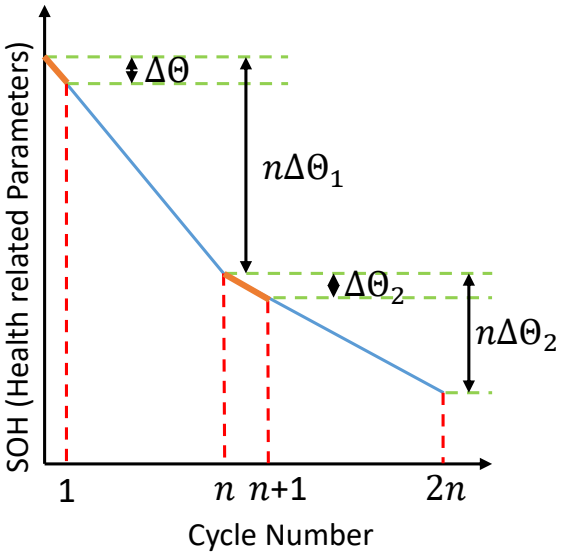

Figure 4: Schematic of the inter-cycle extrapolation algorithm. The change in SOH parameters over one cycle, Δy_1, is assumed to be constant for the next n cycles, resulting in a $n\Delta y_1$ change over n cycles. The change in SOH over the n^{th} cycle is then calculated and extrapolated to the $2n^{\text{th}}$ cycle, etc. Here SOH represents an internal degradation variable of the model, of which there can be several, for example SEI thickness (δ_{SEI}) or active material volume fraction in either electrode ($\varepsilon_{\text{s},k}$).

density, j_{SEI}, and loss of lithium inventory, LLI. There is no visible difference between the two formulations for any of the states.

Figure 3 shows the root mean square percentage error. In each case, the percentage error is well below 1% in all the states. The only exception is $j_{\text{int,n}}$ at the transitions between discharge and rest, and rest and charge, which is due to the two solutions reaching the cut-off discharge voltage at slightly different times. This error is quickly corrected and does not cause error in the other states of interest such as voltage and loss of lithium inventory.

The simulation time with the ODE formulation is three times faster than the DAE formulation, with negligible error. Therefore, we used the ODE formulation to report simulation times in the following section.

4 Adaptive inter-cycle extrapolation

We now present an algorithm to accelerate battery lifetime simulations using adaptive inter-cycle extrapolation. This can be done in conjunction with the reformulation in Section 3, or separately. First, in Section 4.1, we introduce inter-cycle extrapolation and show where this works well and where this fails. We improve on this by making the algorithm adaptive in Section 4.2, and present results in Section 4.3.

4.1 Inter-cycle extrapolation

Battery cycling is a typical example of a process with multiple timescales. The fast timescale is charge/discharge ('cycling'), which occurs on the scale of a few hours and is characterized by the State of Charge (SOC). The slow timescale is degradation, which occurs on the scale of months and is characterized by the State of Health (SOH). State of Health can be assumed to be approximately

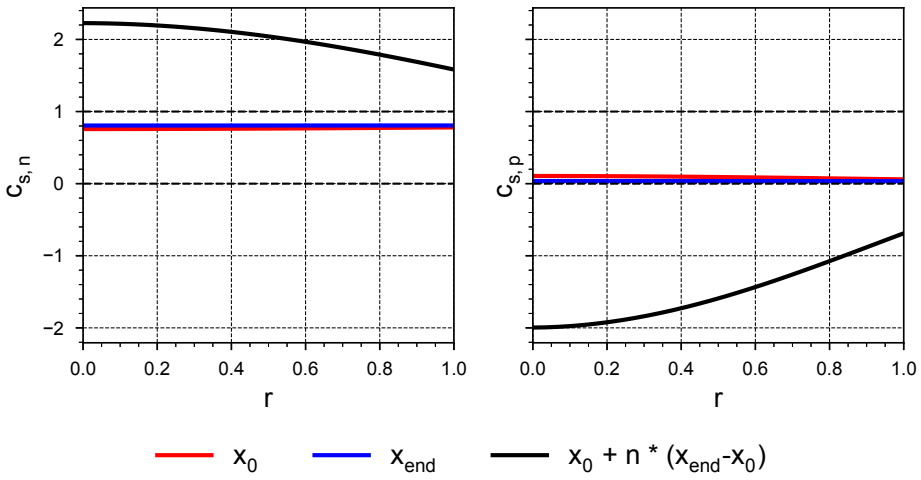

Figure 5: Extrapolating the change from x_0 (red line) to x_{end} (blue line) by n steps leads to an extrapolated value (black line) that is outside of the physical range [0,1] for the dimensionless particle concentration. Therefore, the next cycle cannot be simulated starting from the extrapolated concentration. Here, $n = 30$.

constant over a single cycle, and vary linearly over a few cycles – although there are exceptions at the start and end of life, especially after the 'knee point' [28, 38].

This observation leads to a simple direct extrapolation algorithm for simulating repeated cycles, depicted in Figure 4: run one cycle, measure the change in each state between the beginning and end of simulation, and extrapolate this over several cycles to initialize the next simulation n cycles later,

$$\boldsymbol{x}_0^k = \boldsymbol{x}_{\text{end}}^{k-n} + n\Delta\boldsymbol{x}^{k-n}, \tag{10}$$

$$\Delta\boldsymbol{x}^{k-n} = \boldsymbol{x}_0^{k-n} - \boldsymbol{x}_{\text{end}}^{k-n}. \tag{11}$$

This direct extrapolation algorithm was first proposed for fuel cell models by Mayur et al. [22, 23] as the 'time-upscaling method', and adapted to lithium-ion batteries by Kupper et al. [24]. Vora et al. [25] proposed a similar algorithm at the same time and called it 'extrapolation'. However, the direct extrapolation algorithm is suboptimal, as it requires extrapolating values of 'fine scale' variables such as particle concentration, which can vary quickly on short timescales. Small changes in the value of 'fine scale' variables can lead to large changes after extrapolation, as shown in Figure 5. Instead, only 'coarse scale' variables, which change on longer timescales, should be extrapolated [19]. These variables can be explicit states of the model or aggregated from fine scale variables. In the case of the SPM considered here, (1), we use the coarse scale variables

$$\boldsymbol{y} = [n_{\text{Li,s}}, \delta_{\text{SEI}}, \varepsilon_{\text{s,n}}, \varepsilon_{\text{s,p}}]^T. \tag{12}$$

The three scalar variables δ_{SEI}, $\varepsilon_{\text{s,n}}$, and $\varepsilon_{\text{s,p}}$ are explicit states of the model, but can also be used as coarse scale variables since they change slowly on the degradation timescale (small change over a single cycle. However, we replace the fast-changing particle concentrations $\boldsymbol{c}_{\text{s,n}}$ and $\boldsymbol{c}_{\text{s,p}}$ with the total cyclable lithium, $n_{\text{Li,s}}$, defined as

$$n_{\text{Li,s}} = \frac{3600}{F}\left(\theta_{\text{n}} C_{\text{n}} + \theta_{\text{p}} C_{\text{p}}\right). \tag{13}$$

Details about the total cyclable lithium and related 'degradation modes' are available in Appendix B. Given a total cyclable lithium value, the particle concentrations at full charge (and full discharge) can

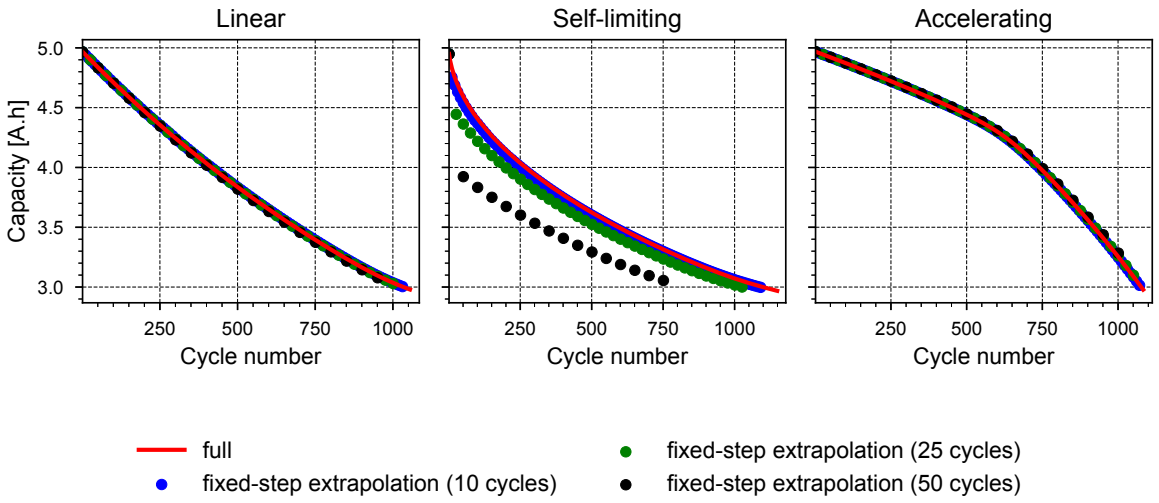

Figure 6: Comparison of the full simulation to the fixed-step extrapolation algorithm. The fixed-step extrapolation algorithm is accurate in the linear and accelerating cases, where the underlying degradation modes are linear (see Section 4.3). In the self-limiting case, where degradation is nonlinear, there is significant error from fixed-step extrapolation, with larger error for larger steps.

be calculated using (25). These are then used to initialize the next simulation after extrapolation. In summary, the fixed step extrapolation algorithm with step size n is as follows:

1. Simulate one cycle from $\boldsymbol{x}_0^{k-n}$ to obtain $\boldsymbol{x}_{\text{end}}^{k-n}$
2. Calculate $\boldsymbol{y}_0^{k-n}$ and $\boldsymbol{y}_{\text{end}}^{k-n}$ using (13)
3. Extrapolate $\boldsymbol{y}$ equivalently to (10) to obtain $\boldsymbol{y}_0^k$
4. Calculate $\boldsymbol{x}_{\text{end}}^k$ using (25) and repeat

Note that if the model contained algebraic states, such as electric potentials, these would not be included in the $\boldsymbol{y}$ vector as they do not require an initial condition and should be automatically initialized by the solver in a way that satisfies the algebraic equations.

In Figure 6 we show the results of using fixed-step inter-cycle extrapolation, comparing three different step sizes (25, 50, and 100) with the full simulation. In the first and third cases, the underlying degradation in mode-space is linear (see Section 4.3). Therefore, the fixed-step extrapolation simulations perform well with any step size, since the assumption that degradation rate remains constant holds. However, in the self-limiting case, the fixed-step extrapolation simulations have significant error, with higher error for larger steps. This is because the rate of degradation decreases rapidly at the start of life, so the extrapolating simulations overestimate the rate of degradation.

4.2 Adaptive algorithm

The results of Figure 6 show that the inter-cycle extrapolation algorithm should take small steps when the rate of degradation changes quickly, and large steps when the rate of degradation is constant. Therefore, instead of extrapolating by a fixed number of cycles each time, we use an adaptive algorithm where the size of the extrapolation step depends on how quickly the rate of degradation is changing.

To do this, we write the degradation system as an ODE

$$\frac{\mathrm{d}\boldsymbol{y}}{\mathrm{d}t} = \Delta\boldsymbol{y}, \tag{14}$$

where the $\boldsymbol{y}$ is defined as in (12). 'Time' is the number of cycles, and $\Delta\boldsymbol{y}$ is the change in $\boldsymbol{y}$ from the start to end of the cycle as observed by simulating the cycle. More specifically, each evaluation of $\Delta\boldsymbol{y}$, as a function of (t and) $\boldsymbol{y}$, consists of the following:

1. Calculate $\boldsymbol{x}_0$ from $\boldsymbol{y}_0 = \boldsymbol{y}$ using (25)
2. Simulate an entire discharge/charge cycle to obtain $\boldsymbol{x}_{\text{end}}$
3. Calculate $\boldsymbol{y}_{\text{end}}$ from $\boldsymbol{x}_{\text{end}}$ using (13)
4. Return $\Delta\boldsymbol{y} = \boldsymbol{y}_{\text{end}} - \boldsymbol{y}_0$

Each evaluation of $\Delta\boldsymbol{y}$ requires solving an entire discharge/charge cycle and thus is relatively expensive.

Equation (14) encodes the degradation that occurs over each cycle into a continuous-time framework that can then be solved by standard numerical integrators. In this context, the fixed-step 'extrapolation' method [22, 23, 24, 25] is the Forward Euler solution. We improve on this by using an adaptive numerical method [39, 40]. Equation (14) is non-stiff, but evaluating the right-hand side is expensive, so we require a method with as few right-hand side evaluations as possible. We use a 3(2) Runge-Kutta algorithm [41] as implemented in SciPy [42]. Since the evolution of the slow timescale ODE is monotonic and almost linear, we use low tolerances (10^{-2} for both relative and absolute tolerance), enabling the ODE solver to take large steps at the required accuracy.

4.3 Results

The cycle-adaptive algorithm is implemented in the open-source battery modeling package PyBaMM [27] and as such can be used with any model in the library. The 'slow' degradation ODE is solved using 3(2) Runge-Kutta in SciPy [42]. Each 'fast' cycle simulation is solved using the method of lines, first discretizing the PDEs spatially using finite volumes with 30 grid points in each particle and then solving the resulting ODE system using CVODE from SUNDIALS via CasADi [33, 34]. The 60% capacity termination condition is implemented as a stopping condition in the 'slow' degradation ODE solver.

Results for the three cases (linear, self-limiting, and accelerating) are shown in Figures 7 to 9 respectively. We show the thermodynamic capacity and stoichiometry limits, calculated using (25), as well as the three degradation modes loss of litihum inventory (LLI) and loss of active material in the negative (LAM_{NE}) and positive (LAM_{PE}) electrodes (see Appendix B for details on degradation modes). In each case, the solid red lines show the full simulation and the dashed blue lines show the adaptive inter-cycle extrapolation simulation, with blue dots showing which cycles were chosen by the adaptive ODE solver to solve the degradation ODE (14). The adaptive inter-cycle extrapolation algorithm accurately captures the evolution of each variable in every case. We now discuss the results of each case in further detail.

In the linear case (Figure 7), the degradation rate is approximately constant and each underlying degradation mode is approximately linear versus cycle number. This leads to approximately linear changes in the capacity and stoichiometry limits, and the adaptive simulation is accurate while able to take a small number of large steps while maintaining accuracy.

In the self-limiting case (Figure 8), the rate of degradation slows down as the cell degrades, driven by self-limiting SEI growth (and hence self-limiting LLI). This effect is most pronounced in the first few hundred cycles. Therefore, the adaptive simulation needs to take small steps at the start of life to resolve the changing rate of degradation, and is able to take larger steps towards end-of-life when degradation becomes more linear. This example demonstrates the power of the adaptive simulation to capture changing degradation rates.

Finally, in the accelerating degradation case (Figure 9), there is a knee point in the capacity fade curve around cycle 600 where capacity fade becomes much faster. Despite this, the adaptive simulation is able to take very large steps. This is because the degradation in mode-space, which is where the extrapolation happens, is approximately linear. Here, the cause of the knee point is that

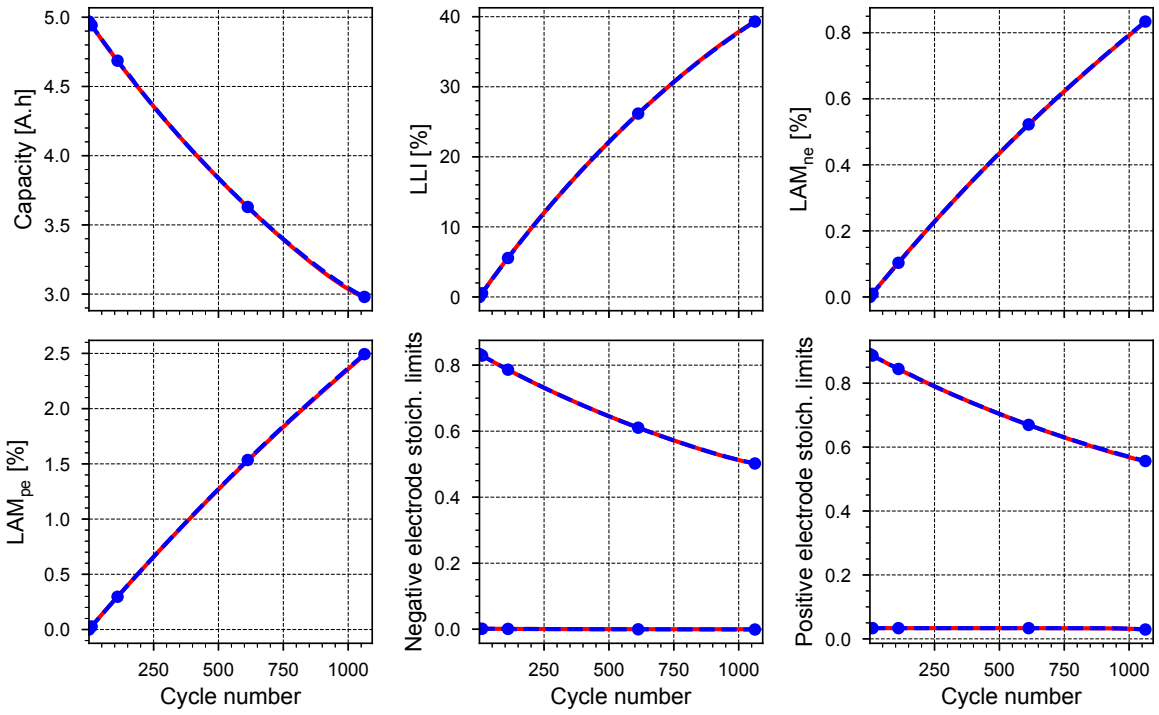

Figure 7: Change in degradation variables during linear degradation. The degradation modes 'loss of lithium inventory' (LLI) and 'loss of active material' (LAM) are defined in Appendix B. The stoichiometry limits are the envelope of the electrode stoichiometry during cycling, which also changes as the battery degrade.

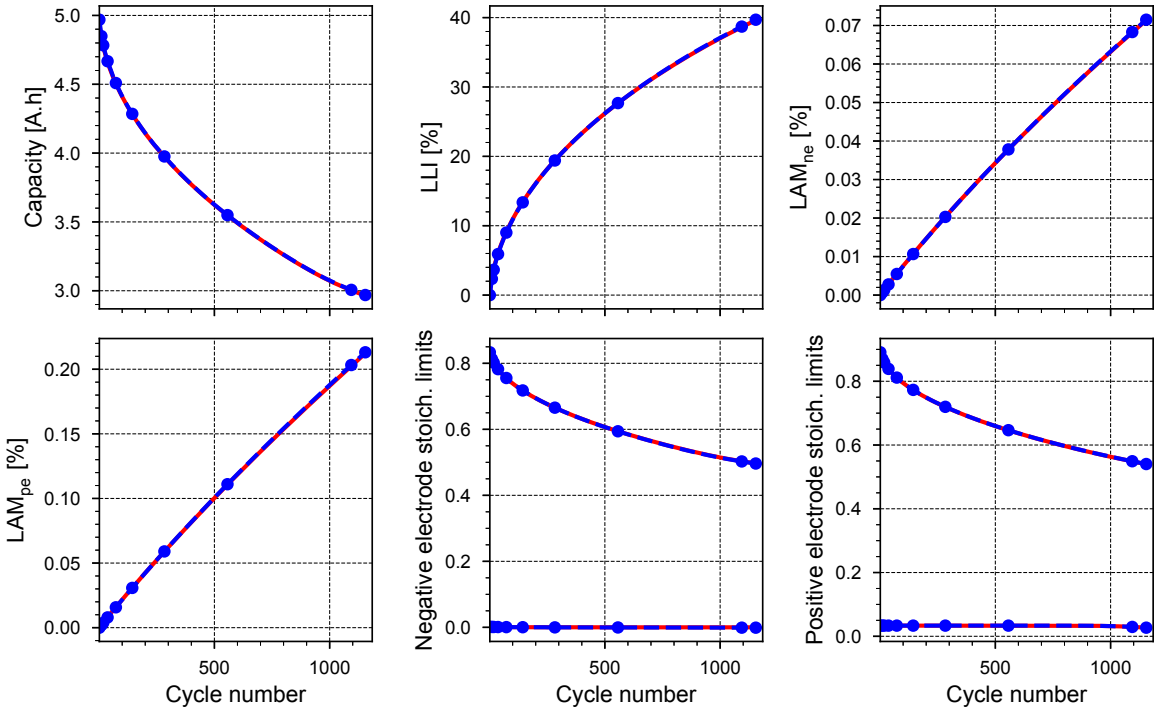

Figure 8: Change in degradation variables during self-limiting degradation (see Figure 7 for details).

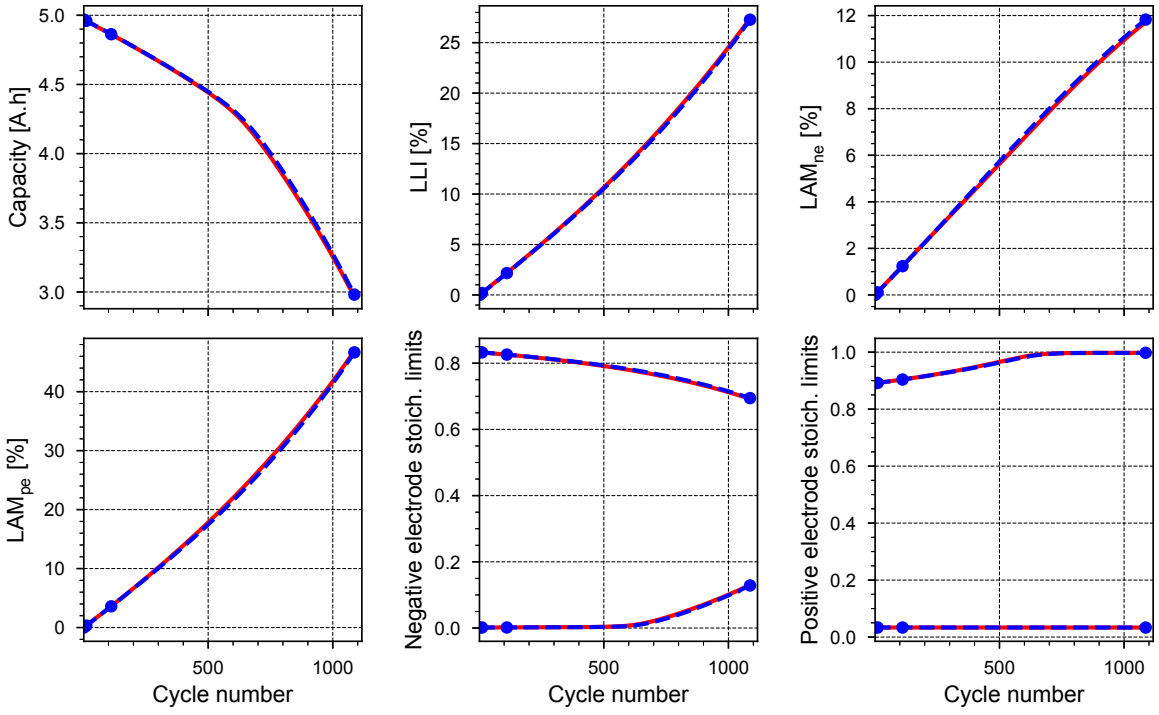

Figure 9: Change in degradation variables during accelerating degradation (see Figure 7 for details)

		Full simulation		Adaptive simulation	
	Cycles to 60%	Cycles solved	Time taken (s)	Cycles solved	Time taken (s)
Linear	1055	1055	173	13	4.5
Self-limiting	1200	1200	178	31	11.2
Accelerating	1085	1085	171	10	3.9

Table 4: Number of cycles solved and time taken for the full and adaptive simulations in each case. The adaptive simulations solve around 20-40 times fewer cycles than the full simulations, since they perform inter-cycle extrapolation, and simulate the entire life of the battery in around 5-10 seconds. Simulations performed on an Apple M1 CPU.

the maximum positive electrode stoichiometry reaches 1 around 600 cycles and cannot go above it, causing a nonlinearity in the minimum electrode stoichiometry limit and the capacity (all of which are related through (25)). This effect has previously been reported in the literature [43].

In summary, for this model, the capacity fade is affected by, firstly, the relative rate of loss of lithium inventory and loss of active material, and secondly, whether the SEI growth is reaction-limited or diffusion-limited. If loss of lithium inventory due to side reactions is faster than loss of active material in both electrodes, so that the utilization of each electrode decreases as the cell ages, degradation is linear or self-limiting. If loss of active material is faster in either electrode, leading to a wider utilization, eventually one of the electrodes will saturate, causing a knee point ('accelerating' capacity fade). Within linear and self-limiting degradation, the capacity fade is approximately linear if the SEI growth is reaction-limited, and the rate slows if the SEI growth is diffusion-limited.

In Table 4, we compare the simulation time for the full simulation and adaptive simulation. The adaptive simulations solve two orders of magnitude fewer cycles, and hence achieve an almost two order of magnitude speed-up. Adaptive simulations can therefore provide almost immediate feedback on a human timescale. We expect the time taken to stay small even when simulating tens of thousands of cycles, since larger steps will be possible in that case. Note that the number of cycles solved by the adaptive simulation is not equal to the number of blue dots in Figures 7 to 9 (roughly three times larger). This is because each blue dot in Figures 7 to 9 requires three cycle evaluations for the third-order adaptive ODE solver used here.

5 Conclusion

In this paper, we have laid the foundations for an adaptive inter-cycle extrapolation algorithm that can simulate the entire lifetime of lithium-ion batteries in a few seconds, and shown the approach to work well in a Single Particle Model with SEI formation and loss of active material. This algorithm will enable researchers to study battery degradation with very rapid feedback on lifetime performance, so that different degradation mechanisms and the coupling between them can better be understood. In this paper, we gain insight into what parameter combinations in a coupled SEI and LAM model cause linear, sublinear, or superlinear capacity fade. In future, the cycle-adaptive simulations can be used to speed up parameter estimation algorithms for determining the parameters of a degradation model, such as those in Table 3.

The main weakness of the cycle-adaptive algorithm is that the extrapolation can only be performed in cases where operating conditions stay constant, such as testing in the lab, and not to simulate batteries in the field where operating conditions vary significantly [1]. Therefore, this algorithm should only be used for improving fundamental understanding of degradation mechanisms, and not to track real batteries in the field.

There are several directions in which this research can be taken to further improve the cycle-adaptive algorithm, and we suggest a few here. First, the algorithm implementation could be improved to allow differentiability with respect to degradation parameters, so that gradient-based methods can be used

for parameter estimation. Second, machine learning surrogates could be used to replace either the 'fast' or 'slow' timescale model, or both. Third, the algorithm could be extended to modeling next-generation chemistries such as lithium metal, for which equations (25) need to be adapted. Finally, as the cycle-adaptive algorithm outputs the cycle numbers selected, this information could be used to make decisions on when to perform reference performance tests for batteries based on the previous trajectory of degradation.

Acknowledgements

This work was supported by the National Science Foundation, Grant Number 1762247 and the University of Michigan Battery Laboratory. We thank Ferran Brosa-Planella and Venkat Viswanathan for insightful discussions.

List of symbols and acronyms

Acroynyms

EC	ethylene-carbonate
LAM	loss of active material
LLI	loss of lithium inventory
SEI	Solid electrolyte interphase

Variables

C	capacity	Ah
I	current	A
J	current	A
$\boldsymbol{N}$	molar flux	mol m^{-2} s^{-1}
V	voltage	V
a	surface area to volume ration	m^{-1}
c	concentration	mol m^{-3}
i	current density	A m^{-2}
j	interfacial current density	A m^{-2}
n_{Li}	lithium inventory	mol
r	radial coordinate	
t	time	
δ	thickness	m
ε_{s}	active material volume fraction	-
η	overpotential	V
ϕ	potential	V

θ	stoichiometry	-
σ	stress	Pa

Parameters

See also Tables 2 and 3

F	Faraday's constant	mol m^{-3}
L	electrode thickness	m
R	ideal gas constant	J mol^{-1} K^{-1}
R_{film}	SEI film resistivity	Ω m
R_k	particle radius	m
U	open-circuit potential	V
i_0	intercalaction exchange-current density	A m^{-2}

Subscripts

e	electrolyte phase
int	intercalation
k	electrode k (n or p)
n	negative electrode
p	positive electrode
s	solid phase
tot	total

Superscripts

surf	at the surface (of particle)
0	leading-order in asymptotic expansion
1	first-order in asymptotic expansion

A SEI kinetics

The model for SEI kinetics from Yang et al. [28] is

$$j_{\text{SEI}} = -F k_{\text{SEI}} c_{\text{EC}}^{\text{s}} \exp\left(-\frac{\alpha_{\text{SEI}} F \eta_{\text{SEI}}}{RT}\right), \tag{15a}$$

$$-D_{\text{SEI}} \frac{c_{\text{EC}}^{\text{s}} - c_{\text{EC}}^{\text{bulk}}}{\delta_{\text{SEI}}} = -\frac{a_{\text{SEI}} j_{\text{SEI}}}{F}. \tag{15b}$$

This is a linear system for j_{SEI} and c^{s}_{EC}, and so we can eliminate the surface concentration of EC, c^{s}_{EC}, to avoid having to solve an additional algebraic equation:

$$\begin{aligned} j_{\text{SEI}} &= \frac{-c^{\text{bulk}}_{\text{EC}}}{1/Fk_{\text{SEI}} \exp\left(-\alpha_{\text{SEI}} F \eta_{\text{SEI}}/RT\right) + a_{\text{SEI}}\delta_{\text{SEI}}/D_{\text{SEI}}F} \\ &= f_{\text{SEI}}(\eta_{\text{SEI}}, \delta_{\text{SEI}}). \end{aligned} \tag{16}$$

The relative size of the two terms in (16) governs the SEI kinetics. If the first term is larger, the SEI growth is reaction-limited. If the second term is larger, the SEI growth is diffusion-limited.

B From degradation mechanisms to degradation modes

Battery degradation can occur through a number of mechanisms, including but not limited to SEI layer growth, lithium plating, mechanical effects in the particles, and electrolyte oxidation [44, 45, 29]. To classify these mechanisms, it is helpful to use degradation modes [44, 45]. The three main degradation modes are loss of lithium inventory (LLI), loss of active material (LAM) in the negative electrode, and LAM in the positive electrode.

Loss of active material is generally caused by mechanical effects. This leads to a reduction in the capacity of the electrodes, C_k:

$$\text{LAM}_k = \left(1 - \frac{C_k}{C_k^{\text{init}}}\right) \times 100 = -\frac{1}{C_k^{\text{init}}} \int_0^t \frac{\mathrm{d}C_k}{\mathrm{d}t}\,\mathrm{d}t \times 100. \tag{17}$$

The charge capacity (in Ah) of the electrodes can be defined as

$$C_k = \frac{\varepsilon_{\text{s},k} A L_k c^{\max}_{\text{s},k} F}{3600}, \tag{18}$$

and so any changes in capacity are caused by changes in active material volume fraction, $\varepsilon_{\text{s},k}$. Degradation models that include LAM usually do so via a differential equation for either the active material volume fraction or electrode capacity.

Loss of lithium inventory is defined as

$$\text{LLI} = \left(1 - \frac{n_{\text{Li,s}}}{n^{\text{init}}_{\text{Li,s}}}\right) \times 100 = -\frac{1}{n^{\text{init}}_{\text{Li,s}}} \int_0^t \frac{\mathrm{d}n_{\text{Li,s}}}{\mathrm{d}t}\,\mathrm{d}t \times 100, \tag{19}$$

where $n_{\text{Li,s}}$ is the total number of moles of cyclable lithium in the particles,

$$n_{\text{Li,s}} = \frac{3600}{F}\left(\theta_{\text{n}} C_{\text{n}} + \theta_{\text{p}} C_{\text{p}}\right), \tag{20}$$

where θ_{n} and θ_{p} are the scaled volumed-averaged negative and positive particle concentrations (or 'electrode stoichiometries') defined in (29). At any time, the total current density in each electrode, j_{tot}, must be equal to the sum of the intercalation density, j_{int}, and the total current density of side reactions, j_{side},

$$j_{\text{tot},k} = j_{\text{int},k} + j_{\text{side},k}, \quad k \in \{\text{n}, \text{p}\}. \tag{21}$$

We define $J_{r,k}$ to be the total current for reaction r in domain Ω_k,

$$J_{r,k} = \int_{\Omega_k} a_{\text{s},k} j_{r,k}\,\mathrm{d}V, \tag{22}$$

This gives the relationship (derived in Appendix C)

$$\frac{\mathrm{d}n_{\text{Li},s}}{\mathrm{d}t} = \frac{\text{I}_{\text{side}}}{F} + \frac{3600}{F}\left(\theta_{\text{n}} \frac{\mathrm{d}C_{\text{n}}}{\mathrm{d}t} + \theta_{\text{p}} \frac{\mathrm{d}C_{\text{p}}}{\mathrm{d}t}\right), \tag{23}$$

and so, by (19), LLI can be decomposed into three parts,

$$\mathrm{LLI} = \underbrace{-\frac{1}{n_{\mathrm{Li,s}}^{\mathrm{init}}}\int_0^t \frac{\mathrm{I_{side}}}{F}\,\mathrm{d}t}_{\mathrm{LLI_{rxn}}} - \frac{3600C_{\mathrm{n}}^{\mathrm{init}}}{Fn_{\mathrm{Li,s}}^{\mathrm{init}}}\underbrace{\frac{1}{C_{\mathrm{n}}^{\mathrm{init}}}\int_0^t \theta_{\mathrm{n}}\frac{\mathrm{d}C_{\mathrm{n}}}{\mathrm{d}t}\,\mathrm{d}t}_{\mathrm{LAM_{liNE}}} - \frac{3600C_{\mathrm{p}}^{\mathrm{init}}}{Fn_{\mathrm{Li,s}}^{\mathrm{init}}}\underbrace{\frac{1}{C_{\mathrm{p}}^{\mathrm{init}}}\int_0^t \theta_{\mathrm{p}}\frac{\mathrm{d}C_{\mathrm{p}}}{\mathrm{d}t}\,\mathrm{d}t}_{\mathrm{LAM_{liPE}}}, \tag{24}$$

where $\mathrm{LLI_{rxn}}$ is the LLI due to side reactions and $\mathrm{LAM_{liNE}}$ and $\mathrm{LAM_{liPE}}$ are loss of lithiated active material, with loss of delithiated active material defined as $\mathrm{LAM_{de}} = \mathrm{LAM} - \mathrm{LAM_{li}}$. Equation (23) shows that loss of lithium inventory occurs not only as a result of side reactions ($\mathrm{I_{side}}/F$) but also as a result of loss of active material ($\mathrm{d}C_k/\mathrm{d}t$).

Some degradation mechanisms, such as pore clogging, do not contribute to either LLI or LAM, but instead to an increase in the internal resistance of the cell. This is sometimes characterized as Ohmic Resistance Increase (ORI), though this term can be misleading as resistance increases can depend nonlinearly on current (for example, if associated with larger concentration gradients due to decreased tortuosity).

It is useful to relate the degradation modes to the stoichiometric limits θ_{n}^0, $\theta_{\mathrm{n}}^{100}$, θ_{p}^0, and $\theta_{\mathrm{p}}^{100}$, where the superscript indicates SOC. For any given $n_{\mathrm{Li,s}}$, C_{n}, C_{p}, and voltage limits $V_{\min}$ and $V_{\max}$, we can find the stoichiometric limits, using the following equations [46]: v

$$n_{\mathrm{Li,s}} = \frac{3600}{F}\left(\theta_{\mathrm{n}}^{100}C_{\mathrm{n}} + \theta_{\mathrm{p}}^{100}C_{\mathrm{p}}\right), \tag{25a}$$

$$C_{\mathrm{n}}(\theta_{\mathrm{n}}^{100} - \theta_{\mathrm{n}}^0) = C_{\mathrm{p}}(\theta_{\mathrm{p}}^0 - \theta_{\mathrm{p}}^{100}), \tag{25b}$$

$$V_{\min} = U_{\mathrm{p}}(\theta_{\mathrm{p}}^0) - U_{\mathrm{n}}(\theta_{\mathrm{n}}^0), \tag{25c}$$

$$V_{\max} = U_{\mathrm{p}}(\theta_{\mathrm{p}}^{100}) - U_{\mathrm{n}}(\theta_{\mathrm{n}}^{100}). \tag{25d}$$

The capacity of the cell is then given by

$$C = C_{\mathrm{n}}(\theta_{\mathrm{n}}^{100} - \theta_{\mathrm{n}}^0) = C_{\mathrm{p}}(\theta_{\mathrm{p}}^0 - \theta_{\mathrm{p}}^{100}), \tag{26}$$

and its State of Charge by

$$z = \frac{Q}{C} = C_{\mathrm{p}}\frac{\theta_{\mathrm{p}} - \theta_{\mathrm{p}}^{100}}{C} = C_{\mathrm{n}}\frac{\theta_{\mathrm{n}}^{100} - \theta_{\mathrm{n}}}{C}. \tag{27}$$

Equation (26) gives the capacity of the cell without needing to simulate a full low C-rate discharge, and equation (27) can be used to initialize a simulation to a given SOC while respecting the balance of lithium and conserving total lithium.

C Loss of lithium inventory

We consider a microscale particle domain Ω_{s} with surface $\partial\Omega_{\mathrm{s}}$, volume V_{s}, and surface area A_{s}, inside a macroscale electrode domain Ω_{tot} with volume $V_{\mathrm{tot}} = AL$. Mass conservation in the particles gives

$$\frac{\partial c_{\mathrm{s}}}{\partial t} = -\nabla\cdot\boldsymbol{N}_{\mathrm{s}}, \qquad \boldsymbol{r}\in\Omega_{\mathrm{s}}, \tag{28a}$$

$$\boldsymbol{N}_{\mathrm{s}}\cdot\boldsymbol{n} = \frac{j_{\mathrm{int}}}{F}, \qquad \text{on } \partial\Omega_{\mathrm{s}}, \tag{28b}$$

where c_{s} is the molar concentration of intercalated lithium, $\boldsymbol{N}_{\mathrm{s}}$ is the flux of lithium in the particles, R_{s} is the particle radius, and j is the intercalation current.

We define electrode stoichiometry to be the particle concentration averaged over both particle domain Ω_{s} and electrode domain Ω_{tot}, and normalized with electrode volume and particle volume:

$$\theta = \frac{1}{AL}\int_{\Omega_{\mathrm{tot}}}\left[\frac{1}{V_{\mathrm{s}}c_{\mathrm{s}}^{\max}}\int_{\Omega_{\mathrm{s}}} c_{\mathrm{s}}\,\mathrm{d}\boldsymbol{r}\right]\mathrm{d}\boldsymbol{x}. \tag{29}$$

Differentiating in time and substituting (28a) gives

$$\frac{\mathrm{d}\theta}{\mathrm{d}t} = \frac{1}{AL}\int_{\Omega_{\mathrm{tot}}}\left[\frac{1}{V_{\mathrm{s}}c_{\mathrm{s}}^{\max}}\int_{\Omega_{\mathrm{s}}} -\nabla\cdot\boldsymbol{N}_{\mathrm{s}}\,\mathrm{d}\boldsymbol{r}\right]\mathrm{d}\boldsymbol{x}, \tag{30}$$

and applying the Divergence Theorem and substituting (28b) gives

$$\frac{\mathrm{d}\theta}{\mathrm{d}t} = \frac{1}{AL}\int_{\Omega_{\mathrm{tot}}}\left[-\frac{A_{\mathrm{s}}j_{\mathrm{int}}}{V_{\mathrm{s}}c_{\mathrm{s}}^{\max}F}\right]\mathrm{d}\boldsymbol{x}, \tag{31}$$

since $A_{\mathrm{s}} = \int_{\partial\Omega_{\mathrm{s}}} 1\,\mathrm{d}S$ and j is uniform over the surface of a particle. Now, if there are N_{tot} particles in the electrode, then by definition

$$\varepsilon_{\mathrm{s}}V_{\mathrm{tot}} = N_{\mathrm{tot}}V_{\mathrm{s}}, \qquad a_{\mathrm{s}}V_{\mathrm{tot}} = N_{\mathrm{tot}}A_{\mathrm{s}}, \tag{32}$$

and so the surface area to volume ratio is related to the porosity through

$$a_{\mathrm{s}} = \frac{\varepsilon_{\mathrm{s}}A_{\mathrm{s}}}{V_{\mathrm{s}}}. \tag{33}$$

For spherical particles, this gives the well-known relation $a_{\mathrm{s}} = 3\varepsilon_{\mathrm{s}}/R_{\mathrm{s}}$. Substituting (33) into (31) gives

$$\frac{\mathrm{d}\theta}{\mathrm{d}t} = -\frac{1}{\varepsilon_{\mathrm{s}}ALc_{\mathrm{s}}^{\max}F}\int_{\Omega_{\mathrm{tot}}} a_{\mathrm{s}}j_{\mathrm{int}}\,\mathrm{d}\boldsymbol{x}, \tag{34}$$

and we can now substitute (22) and (18) to obtain

$$\frac{\mathrm{d}\theta_k}{\mathrm{d}t} = -\frac{J_{\mathrm{int},k}}{3600C_k}. \tag{35}$$

For simplicity, we have assumed ε_{s} to be independent of x, but the derivation can easily be adapted to the case where ε_{s} is a function of x.

We can now find the rate of change of total lithium. Differentiating (20) in time and applying the chain rule gives

$$\frac{\mathrm{d}n_{\mathrm{Li,s}}}{\mathrm{d}t} = \frac{3600}{F}\left(C_{\mathrm{n}}\frac{\mathrm{d}\theta_{\mathrm{n}}}{\mathrm{d}t} + C_{\mathrm{p}}\frac{\mathrm{d}\theta_{\mathrm{p}}}{\mathrm{d}t} + \theta_{\mathrm{n}}\frac{\mathrm{d}C_{\mathrm{n}}}{\mathrm{d}t} + \theta_{\mathrm{p}}\frac{\mathrm{d}C_{\mathrm{p}}}{\mathrm{d}t}\right). \tag{36}$$

Substituting (35), we have

$$\frac{\mathrm{d}n_{\mathrm{Li,s}}}{\mathrm{d}t} = -\frac{1}{F}\left(J_{\mathrm{int,n}} + J_{\mathrm{int,p}}\right) + \frac{3600}{F}\left(\theta_{\mathrm{n}}\frac{\mathrm{d}C_{\mathrm{n}}}{\mathrm{d}t} + \theta_{\mathrm{p}}\frac{\mathrm{d}C_{\mathrm{p}}}{\mathrm{d}t}\right). \tag{37}$$

Now, integrating (21) over the entire electrode gives

$$J_{\mathrm{int,n}} + J_{\mathrm{side,n}} = \mathrm{I}, \tag{38a}$$
$$J_{\mathrm{int,p}} + J_{\mathrm{side,p}} = -\mathrm{I}, \tag{38b}$$

and so, defining the total side reaction current $\mathrm{I}_{\mathrm{side}} = J_{\mathrm{side,n}} + J_{\mathrm{side,p}}$,

$$-\frac{1}{F}\left(J_{\mathrm{int,n}} + J_{\mathrm{int,p}}\right) = \frac{1}{F}\left(J_{\mathrm{side,n}} + J_{\mathrm{side,p}}\right) = \frac{\mathrm{I}_{\mathrm{side}}}{F}. \tag{39}$$

Hence

$$\frac{\mathrm{d}n_{\mathrm{Li,s}}}{\mathrm{d}t} = \frac{\mathrm{I}_{\mathrm{side}}}{F} + \frac{3600}{F}\left(\theta_{\mathrm{n}}\frac{\mathrm{d}C_{\mathrm{n}}}{\mathrm{d}t} + \theta_{\mathrm{p}}\frac{\mathrm{d}C_{\mathrm{p}}}{\mathrm{d}t}\right). \tag{40}$$

References

[1] V. Sulzer, P. Mohtat, A. Aitio, S. Lee, Y. T. Yeh, M. U. Khan, J. W. Lee, J. B. Siegel, A. David, and A. G. Stefanopoulou, "The challenge of battery lifetime prediction from field data," *Joule*, pp. 1–20, 2021.

[2] H. C. Hesse, M. Schimpe, D. Kucevic, and A. Jossen, "Lithium-ion battery storage for the grid - A review of stationary battery storage system design tailored for applications in modern power grids," *Energies*, vol. 10, no. 12, 2017.

[3] A. Bocca and D. Baek, "Optimal life-cycle costs of batteries for different electric cars," *2020 AEIT International Conference of Electrical and Electronic Technologies for Automotive, AEIT AUTOMOTIVE 2020*, no. i, pp. 1–6, 2020.

[4] D. A. Howey, S. A. Roberts, V. Viswanathan, A. Mistry, M. Beuse, E. Khoo, S. C. Decaluwe, and V. Sulzer, "Free Radicals : Making a Case for Battery Modeling," *The Electrochemical Society Interface*, vol. 29, no. 30, 2020.

[5] K. A. Smith, C. D. Rahn, and C. Y. Wang, "Control oriented 1D electrochemical model of lithium ion battery," *Energy Conversion and Management*, vol. 48, no. 9, pp. 2565–2578, 2007.

[6] L. Cai and R. E. White, "Reduction of Model Order Based on Proper Orthogonal Decomposition for Lithium-Ion Battery Simulations," *Journal of The Electrochemical Society*, vol. 156, no. 3, p. A154, 2009.

[7] P. W. C. Northrop, B. Suthar, V. Ramadesigan, S. Santhanagopalan, R. D. Braatz, and V. R. Subramanian, "Efficient Simulation and Reformulation of Lithium-Ion Battery Models for Enabling Electric Transportation," *Journal of The Electrochemical Society*, vol. 161, no. 8, pp. E3149–E3157, 2014.

[8] V. R. Subramanian, V. Boovaragavan, and V. D. Diwakar, "Toward real-time simulation of physics based lithium-ion battery models," *Electrochemical and Solid-State Letters*, vol. 10, no. 11, pp. 255–260, 2007.

[9] P. Barai, K. Smith, C.-F. Chen, G.-H. Kim, and P. P. Mukherjee, "Reduced Order Modeling of Mechanical Degradation Induced Performance Decay in Lithium-Ion Battery Porous Electrodes," *Journal of The Electrochemical Society*, vol. 162, no. 9, pp. A1751–A1771, 2015.

[10] D. Di Domenico, A. G. Stefanopoulou, and G. Fiengo, "Lithium-Ion Battery State of Charge and Critical Surface Charge Estimation Using an Electrochemical Model-Based Extended Kalman Filter," *Journal of Dynamic Systems, Measurement, and Control*, vol. 132, no. 6, p. 061302, 2010.

[11] S. J. Moura, F. B. Argomedo, R. Klein, A. Mirtabatabaei, and M. Krstic, "Battery State Estimation for a Single Particle Model With Electrolyte Dynamics," *IEEE Transactions on Control Systems Technology*, vol. 25, no. 2, pp. 453–468, 2017.

[12] S. G. Marquis, V. Sulzer, R. Timms, C. P. Please, and S. Jon Chapman, "An asymptotic derivation of a single particle model with electrolyte," *Journal of the Electrochemical Society*, vol. 166, no. 15, pp. A3693–A3706, 2019.

[13] F. Brosa Planella, M. Sheikh, and W. D. Widanage, "Systematic derivation and validation of a reduced thermal-electrochemical model for lithium-ion batteries using asymptotic methods," *Electrochimica Acta*, vol. 388, p. 138524, 2021.

[14] I. R. Moyles, M. G. Hennessy, T. G. Myers, and B. R. Wetton, "Asymptotic reduction of a porous electrode model for lithium-ion batteries," *SIAM Journal on Applied Mathematics*, vol. 79, no. 4, pp. 1528–1549, 5 2019.

[15] G. Richardson, I. Korotkin, R. Ranom, M. Castle, and J. Foster, "Generalised single particle models for high-rate operation of graded lithium-ion electrodes: Systematic derivation and validation," *Electrochimica Acta*, vol. 339, p. 135862, 4 2020.

[16] T. L. Kirk, J. Evans, C. P. Please, and S. J. Chapman, "Modelling Electrode Heterogeneity in Lithium-Ion Batteries: Unimodal and Bimodal Particle-Size Distributions," *arXiv*, 2020.

[17] S. G. Marquis, R. Timms, V. Sulzer, C. P. Please, and S. J. Chapman, "A Suite of Reduced-Order Models of a Single-Layer Lithium-Ion Pouch Cell," *Journal of The Electrochemical Society*, vol. 167, no. 14, p. 140513, 2020.

[18] R. Timms, S. G. Marquis, V. Sulzer, C. P. Please, and S. J. Chapman, "Asymptotic reduction of a lithium-ion pouch cell model," *SIAM Journal on Applied Mathematics*, vol. 81, no. 3, pp. 765–788, 2021.

[19] I. G. Kevrekidis and G. Samaey, "Equation-free multiscale computation: Algorithms and applications," *Annual Review of Physical Chemistry*, vol. 60, pp. 321–344, 2009.

[20] G. Wang, "Equation-Free System-Level Modeling and Analytics in Energy Processing Systems," Ph.D. dissertation, Tufts University, 2019.

[21] J. K. Kevorkian and J. D. Cole, *Multiple scale and singular perturbation methods*. Springer Science & Business Media, 2012.

[22] M. Mayur, S. Strahl, A. Husar, and W. G. Bessler, "A multi-timescale modeling methodology for PEMFC performance and durability in a virtual fuel cell car," *International Journal of Hydrogen Energy*, vol. 40, no. 46, pp. 16 466–16 476, 2015.

[23] M. Mayur, B. Weißhar, and W. G. Bessler, "Simulation-based degradation assessment of lithium-ion batteries in a hybrid electric vehicle," in *68th Annual Meeting of the International Society of Electrochemistry, Providence, USA (09/2017) : Book of Abstracts*, ser. 68th Annual Meeting of the International Society of Electrochemistry, Providence, USA (09/2017) : Book of Abstracts, 2017, p. 854.

[24] C. Kupper, B. Weißhar, S. Rißmann, and W. G. Bessler, "End-of-Life Prediction of a Lithium-Ion Battery Cell Based on Mechanistic Aging Models of the Graphite Electrode," *Journal of The Electrochemical Society*, vol. 165, no. 14, pp. A3468–A3480, 2018.

[25] A. P. Vora, X. Jin, V. Hoshing, G. Shaver, S. Varigonda, and W. E. Tyner, "Integrating battery degradation in a cost of ownership framework for hybrid electric vehicle design optimization," *Proceedings of the Institution of Mechanical Engineers, Part D: Journal of Automobile Engineering*, vol. 233, no. 6, pp. 1507–1523, 2019.

[26] L. Trefethen, "Ten digit algorithms," *Mitchell Lecture, June*, no. June, 2005.

[27] V. Sulzer, S. Marquis, R. Timms, M. Robinson, and S. J. Chapman, "Python Battery Mathematical Modelling (PyBaMM)," *Journal of Open Research Software*, vol. 9, no. 1, p. 14, 2021.

[28] X. G. Yang, Y. Leng, G. Zhang, S. Ge, and C. Y. Wang, "Modeling of lithium plating induced aging of lithium-ion batteries: Transition from linear to nonlinear aging," *Journal of Power Sources*, vol. 360, pp. 28–40, 2017.

[29] J. M. Reniers, G. Mulder, and D. A. Howey, "Review and Performance Comparison of Mechanical-Chemical Degradation Models for Lithium-Ion Batteries," *Journal of The Electrochemical Society*, vol. 166, no. 14, pp. A3189–A3200, 2019.

[30] I. Laresgoiti, S. Käbitz, M. Ecker, and D. U. Sauer, "Modeling mechanical degradation in lithium ion batteries during cycling: Solid electrolyte interphase fracture," *Journal of Power Sources*, vol. 300, pp. 112–122, 2015.

[31] W. Ai, L. Kraft, J. Sturm, A. Jossen, and B. Wu, "Electrochemical Thermal-Mechanical Modelling of Stress Inhomogeneity in Lithium-Ion Pouch Cells," *Journal of The Electrochemical Society*, vol. 167, no. 1, p. 013512, 2020.

[32] P. Mohtat, S. Lee, V. Sulzer, J. B. Siegel, and A. G. Stefanopoulou, "Differential Expansion and Voltage Model for Li-ion Batteries at Practical Charging Rates," *Journal of The Electrochemical Society*, vol. 167, no. 11, p. 110561, 2020.

[33] J. A. E. Andersson, J. Gillis, G. Horn, J. B. Rawlings, and M. Diehl, "CasADi – A software framework for nonlinear optimization and optimal control," *Mathematical Programming Computation*, vol. 11, pp. 1–36, 2019.

[34] A. C. Hindmarsh, P. N. Brown, K. E. Grant, S. L. Lee, R. Serban, D. E. Shumaker, and C. S. Woodward, "SUNDIALS: Suite of nonlinear and differential/algebraic equation solvers," *ACM Transactions on Mathematical Software (TOMS)*, vol. 31, no. 3, pp. 363–396, 2005.

[35] M. Safari, M. Morcrette, A. Teyssot, and C. Delacourt, "Multimodal Physics-Based Aging Model for Life Prediction of Li-Ion Batteries," *Journal of The Electrochemical Society*, vol. 156, no. 3, p. A145, 12 2009.

[36] V. Sulzer, S. J. Chapman, C. P. Please, D. A. Howey, and C. W. Monroe, "Faster Lead-Acid Battery Simulations from Porous-Electrode Theory: Part I. Physical Model," *Journal of The Electrochemical Society*, vol. 166, no. 12, pp. A2363–A2371, 2019.

[37] V. Sulzer, "Mathematical Modelling of Lead-Acid Batteries," Ph.D. dissertation, University of Oxford, 2019.

[38] S. Atalay, M. Sheikh, A. Mariani, Y. Merla, E. Bower, and W. D. Widanage, "Theory of battery ageing in a lithium-ion battery: Capacity fade, nonlinear ageing and lifetime prediction," *Journal of Power Sources*, vol. 478, p. 229026, 2020.

[39] R. Rico-Martínez, C. W. Gear, and I. G. Kevrekidis, "Coarse projective kMC integration: Forward/reverse initial and boundary value problems," *Journal of Computational Physics*, vol. 196, no. 2, pp. 474–489, 2004.

[40] S. L. Lee and C. W. Gear, "Second-order accurate projective integrators for multiscale problems," *Journal of Computational and Applied Mathematics*, vol. 201, no. 1, pp. 258–274, 2007.

[41] P. Bogacki and L. F. Shampine, "A 3(2) pair of Runge - Kutta formulas," *Applied Mathematics Letters*, vol. 2, no. 4, pp. 321–325, 1989.

[42] P. Virtanen, R. Gommers, T. E. Oliphant, M. Haberland, T. Reddy, D. Cournapeau, E. Burovski, P. Peterson, W. Weckesser, J. Bright, S. J. van der Walt, M. Brett, J. Wilson, K. J. Millman, N. Mayorov, A. R. Nelson, E. Jones, R. Kern, E. Larson, C. J. Carey, I. Polat, Y. Feng, E. W. Moore, J. VanderPlas, D. Laxalde, J. Perktold, R. Cimrman, I. Henriksen, E. A. Quintero, C. R. Harris, A. M. Archibald, A. H. Ribeiro, F. Pedregosa, P. van Mulbregt, A. Vijaykumar, A. P. Bardelli, A. Rothberg, A. Hilboll, A. Kloeckner, A. Scopatz, A. Lee, A. Rokem, C. N. Woods, C. Fulton, C. Masson, C. Häggström, C. Fitzgerald, D. A. Nicholson, D. R. Hagen, D. V. Pasechnik, E. Olivetti, E. Martin, E. Wieser, F. Silva, F. Lenders, F. Wilhelm, G. Young, G. A. Price, G. L. Ingold, G. E. Allen, G. R. Lee, H. Audren, I. Probst, J. P. Dietrich, J. Silterra, J. T. Webber, J. Slavič, J. Nothman, J. Buchner, J. Kulick, J. L. Schönberger, J. V. de Miranda Cardoso, J. Reimer, J. Harrington, J. L. C. Rodríguez, J. Nunez-Iglesias, J. Kuczynski, K. Tritz, M. Thoma,

M. Newville, M. Kümmerer, M. Bolingbroke, M. Tartre, M. Pak, N. J. Smith, N. Nowaczyk, N. Shebanov, O. Pavlyk, P. A. Brodtkorb, P. Lee, R. T. McGibbon, R. Feldbauer, S. Lewis, S. Tygier, S. Sievert, S. Vigna, S. Peterson, S. More, T. Pudlik, T. Oshima, T. J. Pingel, T. P. Robitaille, T. Spura, T. R. Jones, T. Cera, T. Leslie, T. Zito, T. Krauss, U. Upadhyay, Y. O. Halchenko, and Y. Vázquez-Baeza, "SciPy 1.0: fundamental algorithms for scientific computing in Python," *Nature Methods*, vol. 17, no. 3, pp. 261–272, 2020.

[43] X. Lin, J. Park, L. Liu, Y. Lee, A. M. Sastry, and W. Lu, "A Comprehensive Capacity Fade Model and Analysis for Li-Ion Batteries," *Journal of The Electrochemical Society*, vol. 160, no. 10, pp. A1701–A1710, 8 2013.

[44] C. R. Birkl, M. R. Roberts, E. McTurk, P. G. Bruce, and D. A. Howey, "Degradation diagnostics for lithium ion cells," *Journal of Power Sources*, vol. 341, pp. 373–386, 2 2017.

[45] J. S. Edge, S. O'Kane, R. Prosser, N. D. Kirkaldy, A. N. Patel, A. Hales, A. Ghosh, W. Ai, J. Chen, J. Yang, S. Li, M. C. Pang, L. Bravo Diaz, A. Tomaszewska, M. W. Marzook, K. N. Radhakrishnan, H. Wang, Y. Patel, B. Wu, and G. J. Offer, "Lithium ion battery degradation: what you need to know," *Physical Chemistry Chemical Physics*, vol. 23, no. 14, pp. 8200–8221, 2021.

[46] P. Mohtat, S. Lee, J. B. Siegel, and A. G. Stefanopoulou, "Towards better estimability of electrode-specific state of health: Decoding the cell expansion," *Journal of Power Sources*, vol. 427, no. February, pp. 101–111, 2019.